ACS APPLIED MATERIALS & INTERFACES

Research Article

www.acsami.org

Ultrathin NiGe Films Prepared via Catalytic Solid−Vapor Reaction of Ni with GeH_4

Antony P. Peter,* Karl Opsomer, Christoph Adelmann, Marc Schaekers, Johan Meersschaut, Olivier Richard, Inge Vaesen, Alain Moussa, Alexis Franquet, Tokei Zsolt, and Sven Van Elshocht

Imec, Kapeldreef 75, B-3001 Leuven, Belgium

ABSTRACT: A low-temperature (225−300 °C) solid−vapor reaction process is reported for the synthesis of ultrathin NiGe films (∼6−23 nm) on 300 mm Si wafers covered with thermal oxide. The films were prepared via catalytic chemical vapor reaction of germane (GeH_4) gas with physical vapor deposited (PVD) Ni films of different thickness (2−10 nm). The process optimization by investigating GeH_4 partial pressure, reaction temperature, and time shows that low resistive, stoichiometric, and phase pure NiGe films can be formed within a broad window. NiGe films crystallized in an orthorhombic structure and were found to exhibit a smooth morphology with homogeneous composition as evidenced by glancing angle X-ray diffraction (GIXRD), scanning electron microscopy (SEM), atomic force microscopy (AFM), and Rutherford back-scattering (RBS) analysis. Transmission electron microscopy (TEM) analysis shows that the NiGe layers exhibit a good adhesion without voids and a sharp interface on the thermal oxide. The NiGe films were found to be morphologically and structurally stable up to 500 °C and exhibit a resistivity value of 29 $\mu\Omega$ cm for 10 nm NiGe films.

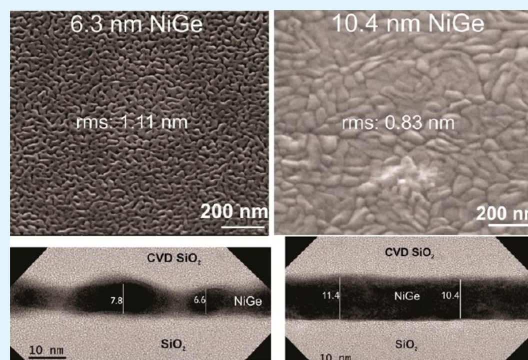

KEYWORDS: *intermetallics, phase identification, reaction synthesis, thin films, physical properties, electron microscopy, scanning, electron microscopy transmission*

INTRODUCTION

Since the inception of integrated circuit (IC) manufacturing, aluminum as a conductor and SiO_2 as an insulator have been the material choice. As the dimensions of the semiconductor devices shrink, the signal propagation speed is limited by resistance capacitance (R-C) delays in the interconnect lines. To lower the RC delay, low resistive metals and low-*k* dielectric constant materials have been introduced.[1] Copper interconnects have been introduced, replacing Al, at the 220 nm technology node.[2] The choice of Cu was due to its reduced electromigration and low resistivity compared to the industry standard Al interconnect material.[3−5] Currently, for the 45 nm technology node, Cu-based interconnects require TaN and Ta barriers to avoid the formation of highly resistive/device detrimental Cu-silicides. Thinning down the interconnect technology further places stringent requirements not only on barriers, seed, and adhesion layers to form a suitable and high-quality interface with Cu but also on the Cu thin film itself that suffers at small dimensions from a major increase of resistivity compared to its bulk value.[6−9] For the technology node extendable to 22 nm or below, a barrierless approach or self-forming barriers would be appropriate as forecasted by International Technology Roadmap for Semiconductors (ITRS). This is mainly due to the fact that at small trenched dimensions (20 nm or below) 2 or 3 nm of barriers and adhesion layers already will occupy substantial volume in the narrow lines leaving less room for conductive metal layers. In addition, at such low thicknesses, the high resistivity of these layers and film nonclosure can be a bottleneck for the downscaling of interconnect technology. Hence, a material that possesses intrinsically low resistivity, grown directly on oxide, without the need for any barriers, but yet showing good adhesion and thermal stability with better electromigration performance, would be the ultimate choice for future interconnect applications.

Reports on ultrathin metal films (≤10 nm, single elements or alloys), especially for interconnect applications, are still lacking in the literature. It is well-known that in the thin-film regime (<15 nm) the metallic layer often tends to break into clusters or islands on oxide surfaces, either during deposition or as a part of the device fabrication process.[10−12] This morphological instability arising due to film dewetting is technologically important in the microelectronics industry, as it can be responsible for the breaking of electrical interconnections. Recently, there has been a report on the resistivity of Ag films in the sub-20 nm regime grown by plasma-assisted atomic layer deposition.[13] Though the bulk resistivity of silver is lower than that of the copper, its chemical stability is a concern. Silver readily oxidizes with sulfur in air leading to an adlayer of Ag_2S limiting its use in many applications.[13] Metal silicides, in last

Received: July 1, 2013
Accepted: August 30, 2013
Published: August 30, 2013

 © 2013 American Chemical Society

two decades, though have been well studied for higher technology nodes,[14] as contact materials the electrical data and film properties for sub-10 nm films are not well established. In addition, compared to silicides, metal germanide thin films are not extensively researched.[15,6] Among the transition metal germanides, NiGe possesses a low resistivity (15 $\mu\Omega$ cm) next only to Cu_3Ge (6 $\mu\Omega$ cm). Unlike nickel silicides, the NiGe system has no equilibrium high-resistivity $NiGe_2$ phase according to the Ni−Ge binary phase diagram. This can avoid the sheet resistance degradation due to phase transformation of low resistive NiGe to $NiGe_2$ during film processing, which is a prime concern for the Ni/Si systems.[16−21]

Recently, we started exploring transition metal germanide thin films, as potential candidates for copper replacement, especially looking for film resistivity in the ultrathin regime (below ≤25 nm). Previously, we reported the film properties and electrical data on thin (20−25 nm) Cu_3Ge layers on TaN/Ta barriers.[22,23] Films were synthesized using catalytic chemical vapor reaction of GeH_4 gas over solid Cu films. Thinning down the Cu_3Ge films resulted in a very rough morphology. The continuity of the layer was found to be influenced by the substrates, remaining more discontinuous-like when grown directly on SiO_2 resulting in high sheet resistance values.[22] In this paper we present the results on smooth and uniform ultrathin NiGe films (≈10 nm), free from voids and agglomeration, grown directly on large-area thermal oxide stacks. The films show self-limiting growth, with a broad process window, and exhibit good interface properties without the need of traditional diffusion barriers and remain structurally stable up to 500 °C, thus showing promise for interconnect applications.

■ EXPERIMENTAL SECTION

For the formation of NiGe layers by solid−vapor reaction, the Ni films were deposited by physical vapor deposition (PVD) at room temperature. Experiments have been performed on 50 nm SiO_2 films grown on 300 mm Si(100) wafers by thermal oxidation. The thickness of the Ni films was varied in the range between 2 and 10 nm to synthesize NiGe layers of different thickness. The GeH_4 (10% in H_2) chemical vapor reactions (also referred to herein as GeH_4 exposure) were carried out along with N_2 at a total chamber pressure of ∼4 Torr.

The phase formation and thickness of the NiGe films were examined by glancing angle X-ray diffraction (GIXRD) (ω = 0.7°) and X-ray reflectivity (XRR) in a Bede MetrixL diffractometer using Cu Kα radiation. The top-view scanning electron microscopy (SEM) analysis was carried out using a Hitachi SU8000 microscope. The morphology of the films was probed using atomic force microscopy (AFM) in tapping mode (model Nanoscope dimension 3100) with an etched single-crystal silicon tip having a radius of curvature <10 nm. The rms roughness of the films was estimated using a scan area size of 2 × 2 μm^2. TEM images were recorded with a FEI Tecnai F30 electron microscope operating at 300 kV, after focused ion beam sample preparation. Energy-dispersive spectroscopy (EDS) and high-angle annular dark field-scanning transmission electron microscopy (HAADF-STEM) data were acquired in parallel. The 4-point probe sheet resistance (Rs) was measured at 49 points across the full wafer, in an Rs100 KLA-Tencor system. Rutherford back-scattering (RBS) analysis was carried out to determine the elemental areal density and the composition of the films using a 1 MeV He+ beam with a sample tilt of 11° and a scattering angle of 170°. Energy-dispersive X-ray spectroscopy (EDX) was carried out using a Philips XL 30 scanning electron microscope at 5 kV equipped with an Oxford Instruments EDX detector. The thermal stability of the NiGe phase was studied using in situ XRD in a purified He atmosphere at a ramp rate of 1 °C/s in the temperature range of 30−500 °C.

■ RESULTS AND DISCUSSION

Previously, NiGe films were targeted, as contact materials, for Ge-based technology, and therefore, the synthetic strategy included solid state thermal reaction of PVD Ni films with different Ge substrates (amorphous, epitaxial, or polycrystalline).[20,24−29] A majority of the studies were focused on the synthesis of thicker NiGe films (50−100 nm) on small sample substrates.[20,24,30−32] Though the NiGe system is less studied, it displays a complexity similar to that of silicide systems. It is well know that controlling the stoichiometry, composition, and crystallographic phase of metal−silicides and −germanides is rather difficult due to the complex phase formation behavior.[33] The phase relations in the Ni−Ge system are very complex due to the existence of several equilibrium phases (NiGe, ε'-Ni_5Ge_3,

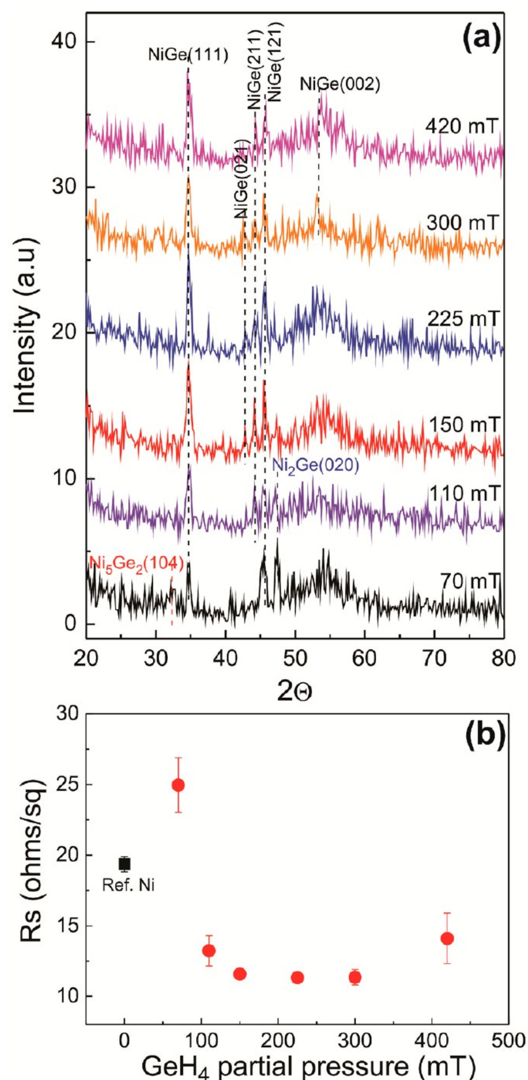

Figure 1. (a) GIXRD spectra for increasing GeH_4 partial pressures on 10 nm Ni films for a 250 °C deposition temperature and 1 min exposure time. The data are offset for clarity. (b) Sheet resistance (Rs) values as a function of GeH_4 partial pressures. The sheet resistance of the reference Ni films is also included in the figure. The error bars are the standard deviation from the 49-point Rs measurements within the full wafer.

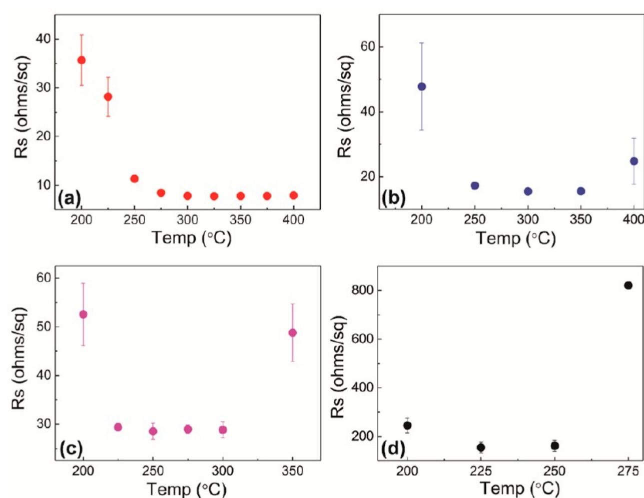

Figure 2. Sheet resistance as a function of GeH_4 exposure temperature for difference thicknesses of Ni. (a) 10 nm Ni, (b) 6 nm Ni, (c) 4 nm Ni, and (d) 2 nm Ni. The partial pressure and exposure time were kept constant (225 mTorr and 1 min). The error bars are the standard deviation from the 49-point Rs measurements within the full wafer.

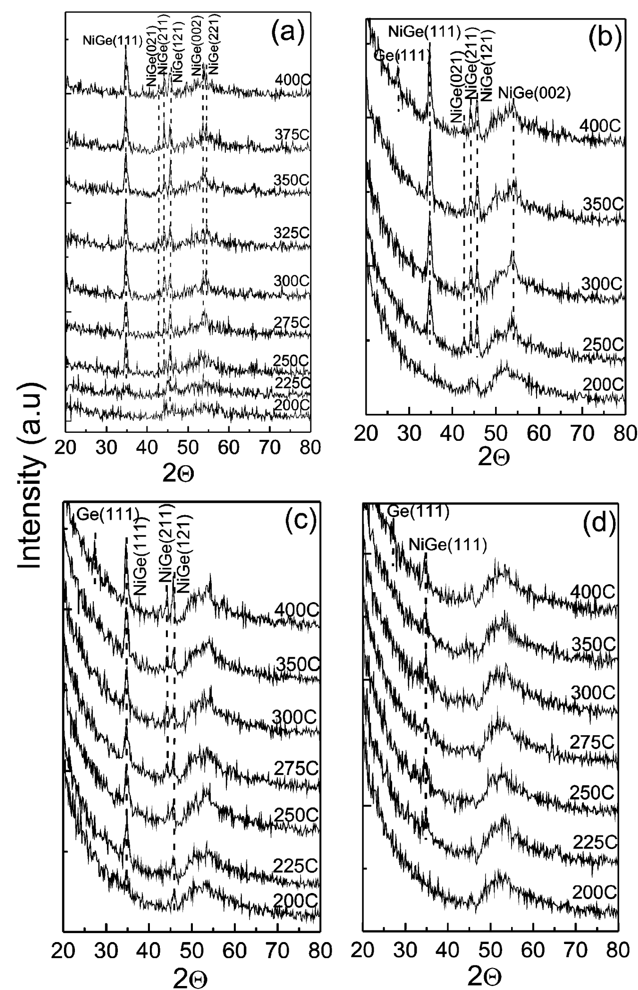

Figure 3. GIXRD spectra for various GeH_4 exposure temperatures for different thicknesses of Ni. (a) 10 nm Ni, (b) 6 nm Ni, (c) 4 nm Ni, and (d) 2 nm Ni. The partial pressure and exposure time were kept constant (225 mTorr and 1 min). The data are offset for clarity.

Ni_2Ge, and Ni_3Ge) and metastable phases (Ni_3Ge_2, $Ni_{19}Ge_{12}$, ε-Ni_5Ge_3, δ-Ni_5Ge_2, and γ-Ni_3Ge).[34,35] Depending on the synthetic strategy, annealing methods, and substrate used, thermodynamically unstable phases (δ-Ni_5Ge_2, ε-Ni_5Ge_3, Ni_3Ge_2) can form, many of which have a higher sheet resistivity.[24,25,36,37] Hence, a thorough understanding and careful tuning of the process conditions are essential to obtain phase pure and high-quality NiGe layers. Especially in the ultrathin regime, agglomeration often results in morphological degradation deteriorating the film sheet resistance as reported in previous solid state thermal processing routes.[21,27] Our approach is different from that of the earlier reports. It relies on the selective chemical vapor deposition (CVD) of the GeH_4 precursor over Ni films and followed by a diffusion reaction leading to NiGe thin films at very low temperatures compatible to the back-end-of-line (BEOL) technology for device fabrication.

The manuscript is organized as follows: First, the optimization of the solid−vapor reaction conditions (GeH_4 partial pressure, exposure temperature, and time) for different thicknesses of Ni (10−2 nm) is presented with the goal to identify the conditions favorable for the formation of phase pure and low resistive NiGe films. This is followed by a detailed analysis of such synthesized layers of different thicknesses, to elucidate the NiGe film properties (film closure, uniformity, roughness, and volume expansion) and thermal stability.

Figure 1a shows the GIXRD spectra studied as a function of GeH_4 partial pressure. The initial Ni thickness was 10 nm. The deposition temperature and time were kept constant to 250 °C and 1 min, respectively. The partial pressure experiments were carried out at a fixed chamber pressure but by varying the flow of GeH_4/H_2 and N_2 gas. At 70 mTorr GeH_4, the peaks correspond to a Ni_2Ge + NiGe + Ni_5Ge_2 mixed phase. At 110 mTorr GeH_4, the Ni_5Ge_2 peak [PDF. No: 00-024-0451] disappears, and the spectrum consists of Ni_2Ge [PDF. No: 01-071-5486] with reduced intensity together with dominating NiGe peaks. In the partial pressure range of 150−420 mTorr GeH_4, the peaks due to (111), (021), (211), (121), and (002) reflections correspond to phase pure orthorhombic NiGe [PDF. No: 01-089-7084], and no traces of other Ni−Ge structures are evidenced. Figure 1b shows the sheet resistance (Rs) values measured for each partial pressure studied. The Rs value (19.37 ± 0.54 Ω/sq) of the reference Ni films is also included in the figure for comparisons. A clear difference in Rs values can be observed after the GeH_4 chemical vapor reaction with Ni. Consistent with the GIXRD phases formed, the Rs values were found to be high for the lower partial pressure (≤110 mTorr GeH_4) due to incomplete reaction. Constant Rs values (∼11 Ω/square) were noted in the partial pressure range 150−320 mTorr where the phase corresponds to that of NiGe. A slight increase of the Rs value (14.11 ± 1.79) at 420 mTorr could probably be related either to traces of Ge incorporation, which GIXRD could not index, or to the rough film morphology.[22,23]

Figure 2a−d represents the change in sheet resistance as a function of GeH_4 exposure temperature for different thicknesses of Ni (10−2 nm). The exposure time (1 min) and GeH_4 partial pressure (225 mTorr) were kept constant. The partial pressure was chosen based in Figure 1, i.e., the range where low resistive NiGe films were obtained. From Figure 2, it is clearly evident that except for the 10 nm case the impact of CVD temperature on the sheet resistance is similar. For 10 nm Ni, the Rs value drops initially, when the temperature is increased

dx.doi.org/10.1021/am4024719 | ACS Appl. Mater. Interfaces 2013, 5, 9605−9614

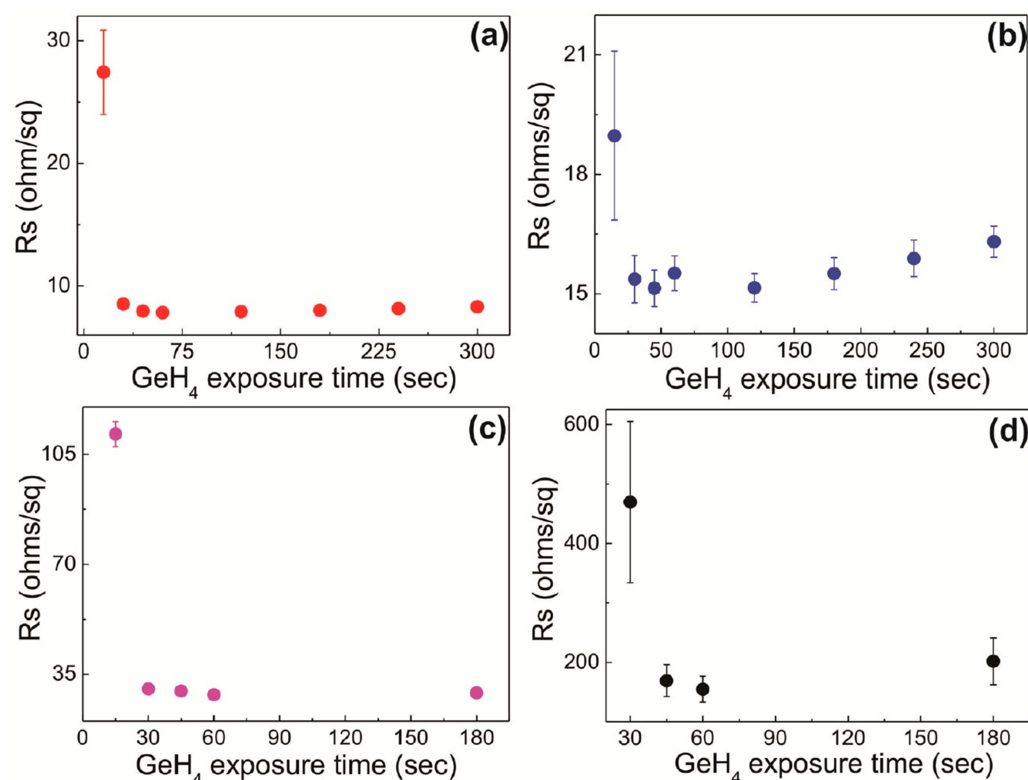

Figure 4. Sheet resistance as a function of GeH_4 exposure time for different thicknesses of Ni. The GeH_4 vapor reaction temperature depends on the film thickness (a) 10 nm Ni, 300 °C; (b) 6 nm Ni, 300 °C; (c) 4 nm Ni, 250 °C; and (d) 2 nm Ni, 225 °C. The partial pressure of germane is kept constant (225 mTorr). The error bars are the standard deviation from the 49-point Rs measurements within the full wafer.

from 200 to 275 °C, and remains constant (~7.8−7.9 Ω/sq) with a broad temperature window (275−400 °C). In contrast, for the Ni film thicknesses in the range 6−2 nm, it can be observed that the temperature window to realize a stable Rs value gets narrower (6 nm Ni: 250−350 °C; 4 nm Ni: 225−300 °C; and 2 nm Ni 225−250 °C). The Rs value increase for higher temperatures, for the thinner Ni films, is probably associated either to the excess Ge incorporation or to the morphological instability of the grown NiGe films.

Figure 3 shows the GIXRD traces of NiGe films synthesized at various temperatures (200−400 °C) using different thicknesses of Ni (10−2 nm) but with a fixed GeH_4 partial pressure (225 mTorr) and exposure time (1 min). The impact of temperature during GeH_4 exposure on the NiGe phase formation is comparable for all thicknesses. Below 225 °C, the GeH_4 reaction with Ni does not occur. Above the temperature, peaks corresponding to NiGe can be observed. With the exception of 10 nm Ni, the presence of minor Ge is noticed for the rest of the Ni film thicknesses studied at 400 °C. Considering the GIXRD patterns that remain the same for the 4 and 2 nm Ni start layers, for all the temperatures investigated the different Rs behavior noted at higher temperatures (Figure 2) confirms that the morphological instability would be the cause for the tremendous increase of Rs values beyond 300 and 250 °C. The fact that the Rs cannot be measured for the films grown at 400 and 300 °C using 4 and 2 nm Ni clearly confirms this. This is line with the previous reports on NiGe films synthesized using solid state anneal routes, where agglomeration or layer breakage was found to be prevalent, for lower thicknesses, at higher temperatures.[27,21] Combining GIXRD results with that of Rs, the following GeH_4 reaction temperatures were chosen: 300 °C for 10 and 6 nm Ni and 250 and 225 °C for 4 and 2 nm Ni to study the impact of GeH_4 exposure time, since low resistive NiGe films are formed at these temperatures.

In Figure 4a−d we plot sheet resistance as a function of GeH_4 chemical vapor reaction time for different thicknesses of Ni. For all thicknesses investigated, the same trend can be observed. Initially, a high Rs value is observed which drops to a constant low value for exposure times of 15 s and beyond. Unlike the temperature window, which was found to be dependent on Ni thickness, the exposure time is not that critical above 15 s and roughly independent of thickness. Figure 5a−d shows the GIXRD transformation as a function of GeH_4 exposure time for all the Ni thicknesses (10−2 nm). Consistent with the Rs data, the lower exposure time (15 s) results in either the formation of Ni-rich germanides or an incomplete reaction. For exposure times where the Rs was found to be low and stable, the GIXRD corresponds to that of phase pure NiGe formation. Also, the reduction in the number of NiGe reflections with thickness indicates a lower crystallinity for thinner NiGe films.

The larger Rs and phase window with GeH_4 exposure time is also extended to the uniform film morphology, as shown by the SEM analysis. Figure 6 shows the SEM morphology for reaction time starting from a 10 nm Ni film. The as-deposited Ni film had a flat and featureless morphology (Figure 6a). A clear distinction in surface morphology could be noticed after its reaction with GeH_4 precursor. Barring the 15 s exposure (Figure 6b), the film morphology was found to be similar, exhibiting compact-like grainy structures for all the exposure times studied (Figure 6c−f). Patches of clusters, driven by nucleation and aggregation, noted for 15 s exposure time show the onset of the GeH_4 chemical vapor reaction with Ni.

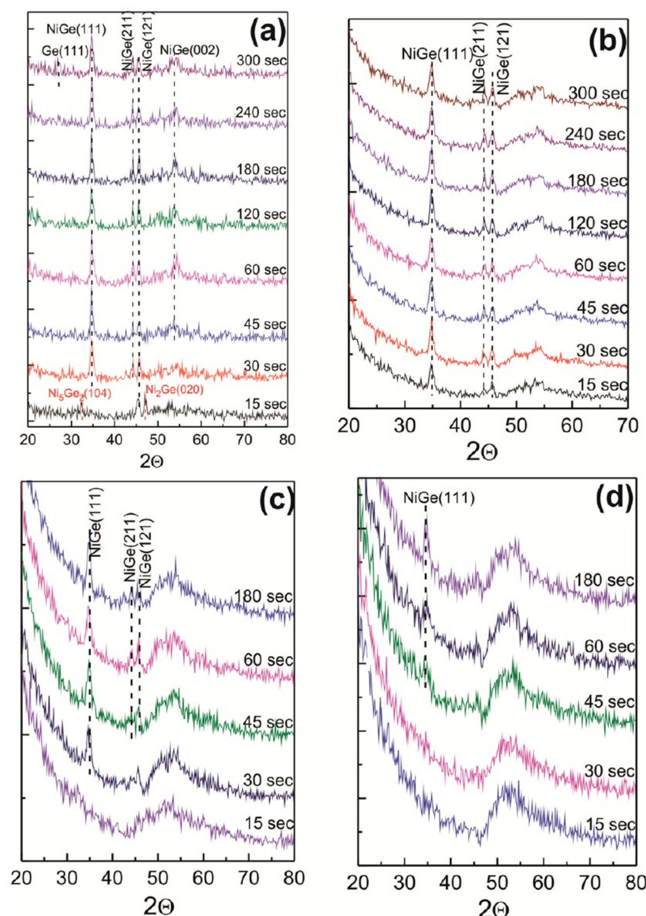

Figure 5. GIXRD patterns for various GeH_4 exposure times for different thicknesses of Ni. The solid−vapor temperature depends on the film thickness. (a) 10 nm Ni, 300 °C; (b) 6 nm Ni, 300 °C; (c) 4 nm Ni, 250 °C; and (d) 2 nm Ni, 225 °C. The partial pressure of germane is kept constant (225 mTorr). The GIXRD traces are offset for clarity.

To further complement the GIXRD, Rs, and SEM analysis, the stoichiometry was anaylsed by RBS. The measured Ni to Ge ratio is 1:1 corresponding to the mononickel germanide (NiGe) for the films after 30−120 s GeH_4 exposure time. The film grown at 15 s exposure time was Ni-rich (Ni/Ge = 1.37). Higher GeH_4 exposure times in the region (180−300 s) were found to be slightly rich in Ge content (Ni/Ge = 0.93), yet only resulting in a negligible increase in sheet resistance (Figure 4a) and a homogeneous morphology (Figure 6f). The NiGe system demonstrates a much broader window for the solid−vapor reaction process as compared to the Cu_3Ge film synthesized using the same approach.[22,23] Even a short increase of GeH_4 exposure time from 30 to 60 s for 10 nm Cu was found to deteriorate the Cu_3Ge film quality and electrical properties, resulting in a large increase in sheet resistance values due to the nonuniform film morphology and excess Ge incorporation.[22] Despite the absence of the Ge-rich germanide phase beyond NiGe and Cu_3Ge for both the Ni/Ge and Cu/Ge systems,[34,38] the introduction of surplus Ge remaining sensitive only for Cu possibly arises due either to the faster Ge diffusivity in Cu (6.80×10^{-11} cm^2/s) than in Ni (1.48×10^{-25} cm^2/s) or to the differences in Ge solubility and catalytic effects at the opted solid−vapor reaction temperature.[39]

We further studied the surface roughness, layer closure, volume expansion after solid−vapor reaction, film resistivity, and thermal stability for NiGe films with different thicknesses. Taking advantage of the Rs and GIXRD phase window which was found to be broad and hardly was influenced by the GeH_4 exposure time (Figures 4 and 5), for all the Ni thicknesses studied, the NiGe films that were prepared with the following conditions: 10 nm Ni, 45 s; 6 nm Ni, 45 s; 4 nm Ni, 60 s; 2 nm Ni, 60 s, were chosen for the detailed analyses, as a proof of concept. Figure 7 shows the AFM morphology and rms roughness analysis of the NiGe films derived from the different thicknesses of Ni (2−10 nm). The optimal growth conditions (GeH_4 exposure time and temperature) of these layers are also given in the figure. From the AFM morphology (Figure 7a−d)

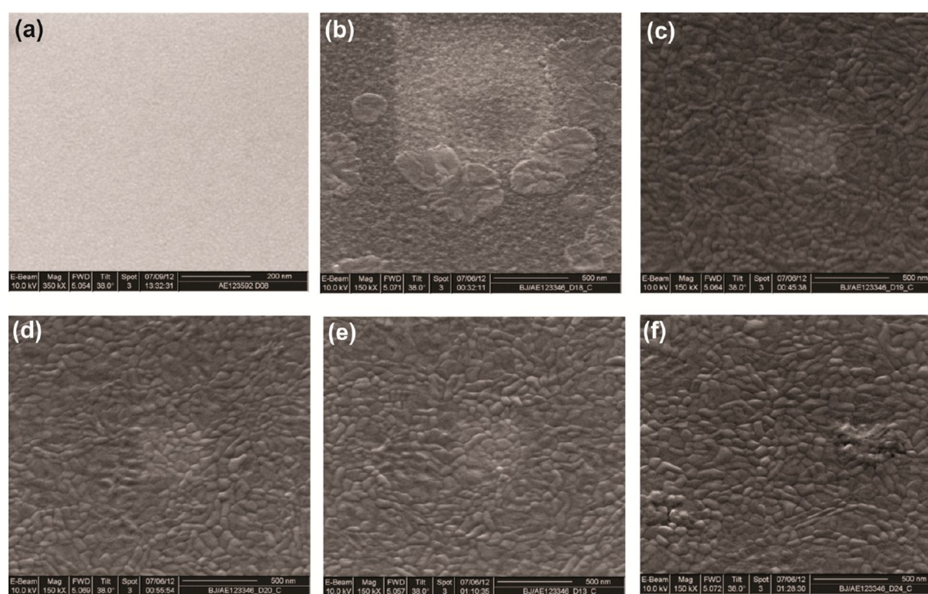

Figure 6. Representative SEM morphology of 10 nm PVD Ni films before and after solid−vapor reaction with GeH_4 at different exposure times. (a) 0 s, reference untreated Ni, (b) 15 s, (c) 30 s, (d) 45 s, (e) 60 s, and (f) 300 s. The GeH_4 exposure temperature and partial pressure were kept constant at 300 °C and 225 mTorr, respectively.

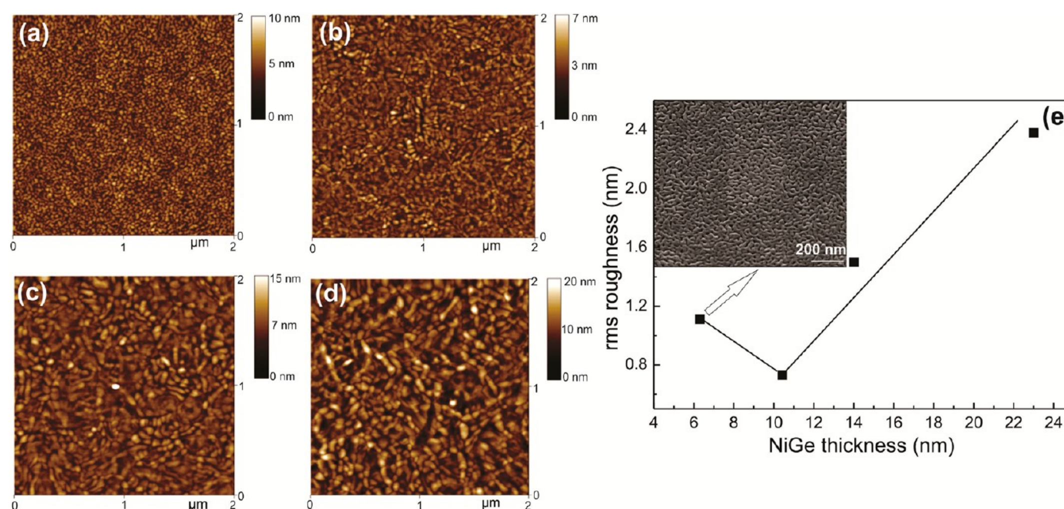

Figure 7. (a)−(d) AFM morphology of NiGe films synthesized from different thicknesses of Ni with the respective GeH_4 exposure time and temperature. (a) 2 nm Ni (60 s, 225 °C); (b) 4 nm Ni (60 s, 250 °C); (c) 6 nm Ni (45 s, 300 °C); (d) 10 nm Ni (45 s, 300 °C). (e) AFM rms roughness against the NiGe thickness. The inset represents the SEM top-view morphology of the NiGe films prepared from 2 nm Ni.

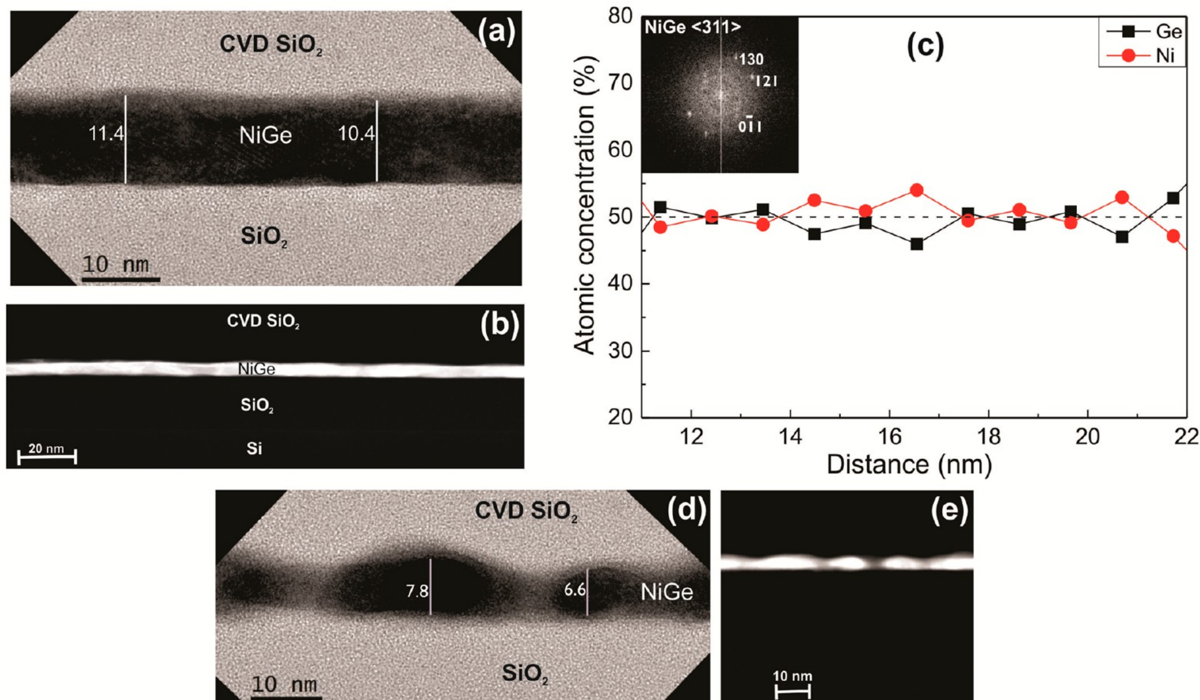

Figure 8. (a),(b) TEM cross-sectional and dark-field STEM image of NiGe films synthesized from 4 nm Ni. (c) EDS elemental composition across the thickness of the NiGe layers. The inset shows the electron diffraction pattern derived from the NiGe layers. (d),(e) TEM cross-sectional and HAADF-STEM image of NiGe films synthesized from 2 nm Ni.

derived from the 2 × 2 μm^2 scans, the increase in grain growth with thickness could be clearly evidenced, in agreement with the GIXRD results that showed an increase in NiGe peaks with Ni thickness. The rms roughness values, in agreement with the film crystallinity trend, confirmed an increase of film roughness with NiGe thickness, except for the films grown using 2 nm Ni. The thickness of the NiGe films was estimated from the XRR and TEM analysis, the results of which will be discussed in the coming sections. Though the AFM scans on the NiGe film grown from 2 nm Ni showed a morphology consisting of small grainlike structures, the fact that its rms roughness value is higher than the NiGe film grown from 4 nm Ni (1.11 vs 0.83 nm) suggests that the layers are not closed. To confirm that SEM and TEM analyses were extended, SEM top-view morphological analysis showed that the NiGe films (~6 nm) grown from 2 nm Ni films (Figure 7e, inset) consist of isolated grainlike structures, indicating the layers are not closed.

TEM analysis was carried out on the NiGe films grown using 4 and 2 nm Ni, the results of which are presented in Figure 8. Figure 8a shows the cross-sectional TEM image of NiGe films (from 4 nm Ni) exhibiting a sharp and planar interface with the underlying thermal oxide surfaces. No new interphase formation, morphological instability, or voids noted shows the films to have good adhesion with the oxide surface. The 4

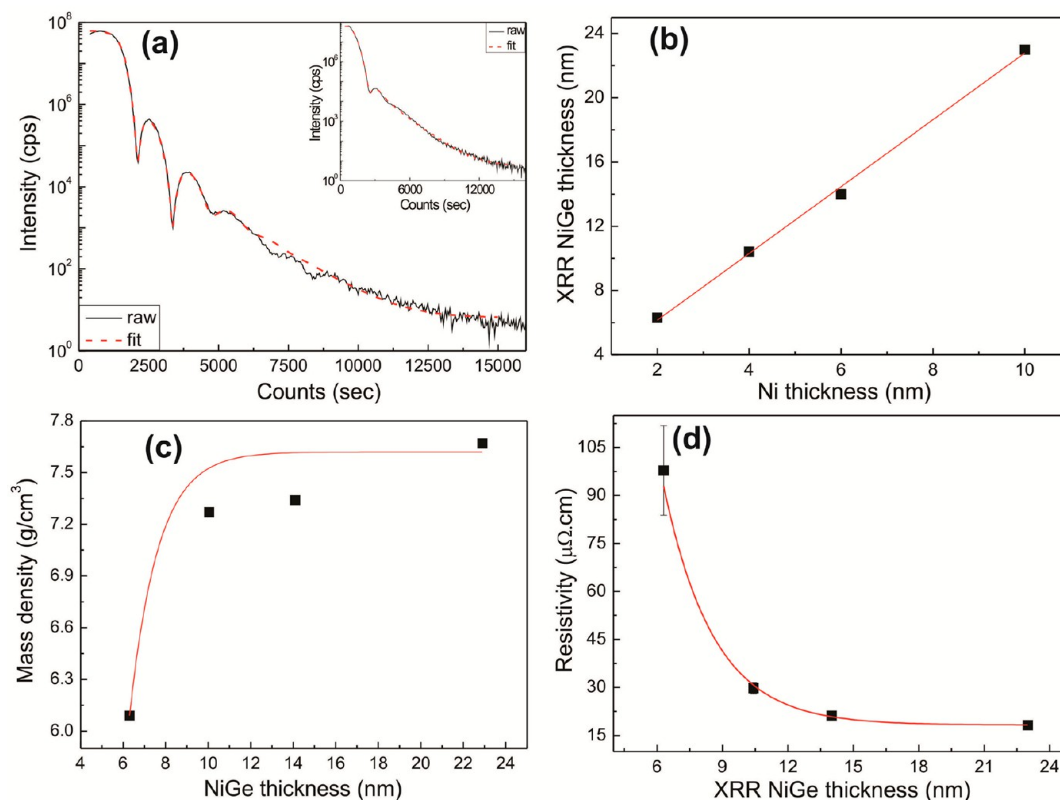

Figure 9. (a) XRR traces of NiGe layers from 4 nm Ni. The inset shows the XRR curve of NiGe from 2 nm Ni. (b) Plot of NiGe layer thickness after chemical vapor reaction vs initial Ni film thickness. (c),(d) NiGe film mass density and resistivity as a function of XRR thicknesses. The errors for the Ni and NiGe thickness from XRR across the wafer are <1%, and the uncertainty of the (atom) areal density determined from RBS is <5%. The trend line in the mass density is provided as a guide to the eye.

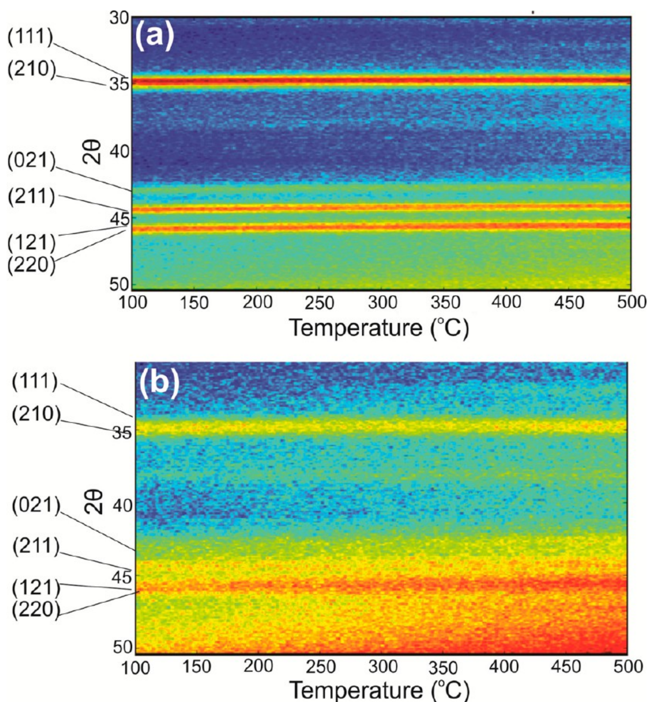

Figure 10. In situ XRD of NiGe films of selected thicknesses synthesized using the optimal solid−vapor reaction conditions: (a) 23 nm, 45 s exposure at 300 °C and (b) 10 nm, 60 s exposure at 250 °C. The blue color indicates the lowest intensity due to background, and the red shows the highest intensities from the diffraction peaks.

nm Ni film reacts to 10.5 nm NiGe. Figure 8b depicts the HAADF-STEM image of NiGe layers showing a homogeneous contrast throughout the thickness indicating no variation in film composition. This was also complemented by the dark-field STEM analysis that showed a uniform contrast in film density and crystallinity (results not shown). The EDS line profile on the film composition carried out through the thickness of NiGe films is given in Figure 8c. The average compositional analysis performed at eight different points showed a uniform profile consisting of 49.6 Ge% and 50.4% Ni consistent with the STEM analysis indicating that the Ni film is totally transformed under the optimized conditions and leads to homogeneous and stoichiometric NiGe films. Fast Fourier transformation (FFT) patterns obtained from the high-resolution images showed the films to be polycrystalline. The electron diffraction pattern could be indexed to orthorhombic NiGe lattices (space group: pbnm, a = 0.5381, b = 0.5811 and c = 0.3428, $\alpha = \beta = \gamma = 90°$) similar to that of GIXRD findings. A typical diffraction pattern obtained from the 10 nm NiGe films is given in the inset of Figure 8c. Figure 8d presents the cross-section TEM image of NiGe films grown from 2 nm Ni films. From the contrast, one could clearly see a vacant-like region between the dark grains, suggesting the layer is not closed. This is further supported by the HAADF-STEM image that showed the contrast difference due to empty regions and NiGe grains (Figure 8e).

XRR analysis was performed to extract the NiGe film thickness, mass density, and volume expansion after the solid−vapor reaction. Figure 9a presents the representative experimental and simulated XRR curves for the NiGe films grown using 4 nm Ni, and the inset shows that of films prepared from

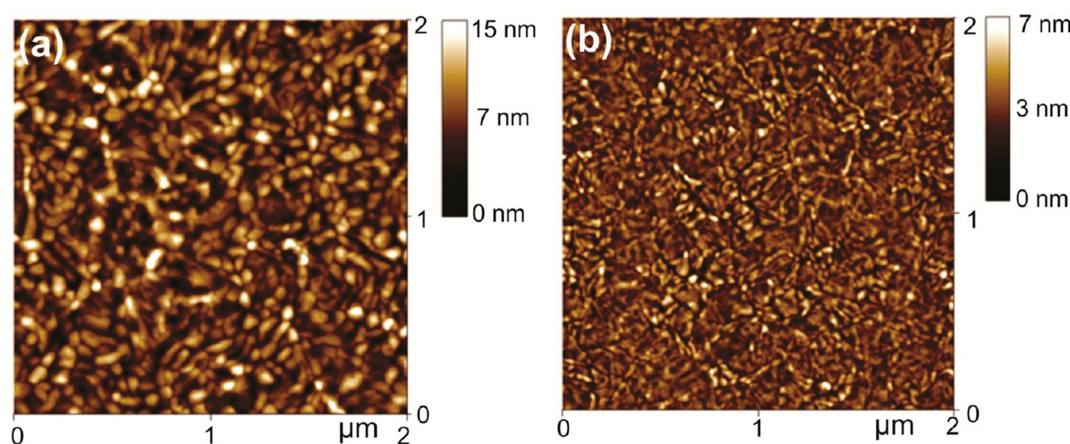

Figure 11. AFM morphologies of NiGe films of different thicknesses after anneal at 500 °C in He ambience. (a) 23 nm and (b) 10 nm NiGe films synthesized from 10 and 4 nm Ni at a GeH_4 exposure time of 45 and 60 s at 300 and 250 °C, respectively.

2 nm Ni film. The reduction in number of fringes for the films grown with 2 nm Ni is clearly indicative of the lower NiGe thickness obtained, compared to the case of 4 nm Ni. Best fits to these and to the ones grown using 6 and 10 nm Ni (results not shown) yielded a value of 6.3, 10.4, 14, and 23 nm as thickness for NiGe films. This when plotted against the initial Ni film thickness (Figure 9b) gives a value of 2.08 ± 0.06 as a slope, indicating that one unit volume of Ni consumes 1.08 times its volume of the Ge from GeH_4 gas and forms NiGe films with a total volume expansion of 2.08 times that of Ni. The theoretical volume expansion for germane vapor reaction with Ni is found to be 3.08, based on the theoretical Ni and Ge bulk density. The thickness ratio (2.08) of NiGe films obtained from the current study is lower compared not only to the theoretical volume expansion but also to the other rapid thermal anneal route processed NiGe thin films where a ratio of 2.55 is reported.[16,21,27] It should be highlighted that despite the large volume expansion the films remain intact and smooth with no agglomeration or grooving noticed, except for the thinnest NiGe film (6.3 nm) which was discontinuous.

The thickness derived from the XRR is in good agreement with that of TEM results. Mass density calculated from XRR thickness and RBS area density is provided in Figure 9c. It is obvious that the 6.3 nm NiGe films, being not closed, possess low density (6.1 g/cm^3). Beyond this point, the density increases with thickness reaching a value of 7.7 g/cm^3 for 23 nm thick NiGe films. Figure 9d shows the thickness vs resistivity curve for the NiGe films, synthesized under optimized conditions. The sharp increase in resistivity below 10 nm, showing an exponential like trend, is due to the film discontinuity. For a thickness of 10 nm, a resistivity value of 29 $\mu\Omega$ cm is measured, which reasonably matches with that of values (22−25 $\mu\Omega$ cm) reported in the literature but for higher NiGe film thicknesses (25−70 nm) processed via solid state reaction routes.[28,40,41] The resistivity is comparable to that of atomic layer deposited 10 nm Ru films (25−35 $\mu\Omega$ cm) reported recently, the growth of which was found to be feasible only with TiN or TaN seed layers.[7,42]

In the current interconnect technology nodes, Cu agglomeration or dewetting on oxide surfaces is avoided by introducing Ta/TaN metallic barriers.[43] With the downscaling of the technology to16 nm or beyond, it is imperative to avoid barrier layers, as it adds not only to the line resistance, owing to their higher resistivity than Cu, but also to the difficulties in depositing continuous barrier layers (1−2 nm).[6] NiGe films deposited directly on oxides will be beneficial in terms of both intrinsic resistivity, with no contribution from the underlying layers, and no interface related issues with adhesion and diffusion barrier layers as observed for Cu-based systems.[44] Another notable advantage with the NiGe system, compared to the Cu-based ones, is that the films are synthesized without any plasma pretreatment, to remove the native oxide, which potentially can minimize the problems associated with the damage of ultralow *k* materials for advanced interconnect developments.[45,46]

It should be mentioned here that at the opted reaction temperatures (225−300 °C) to synthesize NiGe films of different thicknesses GeH_4 undergoes selective and catalytic CVD on Ni[39,47,48] since no GeH_4 decomposition on thermal oxide up to 350 °C was observed, based on GIXRD results (data not shown). This is further supported by the previous GeH_4 CVD reports wherein the pyrolysis leading to Ge films is demonstrated at 400 °C or above.[49,50] This low-temperature processing of NiGe films via a catalytic decomposition-cumene-reaction is crucial for the integration into interconnect structures, where process temperatures of 400−450 °C would be detrimental to the underlying low-*k* materials used in BEOL technology.[51]

To study the NiGe thermal stability, films of selected thicknesses (23 and 10 nm) prepared under ideal growth conditions were subjected to temperature anneals (100−500 °C), and in situ XRD was recorded simultaneously during ramping. Figure 10 shows the in situ XRD data collected from the NiGe films during a thermal ramp (0.2 °C/s), in an inert He atmosphere. Figure 10(a),(b) shows the XRD intensity contour maps plotted as a function of anneal temperature for 23 and 10 nm NiGe films. It is clear from XRD results that the observed diffraction peaks could be related to the NiGe phase throughout the investigated temperature range (Figure 10a). No new peaks due to Ge, GeO_2, or nickel silicidation, nor a decay in the intensity of the NiGe peaks, demonstrates that NiGe is structurally stable up to 500 °C. Similar results were noted on the thinner NiGe films (Figure 10b), though peak intensities are lower due to weak crystallinity compared to the thicker films. The morphology and roughness of the films quenched after the 500 °C anneal are presented in Figure 11. It can be seen from the images that no morphological degradation is noted, after the anneal, for both film thicknesses. An rms

roughness value of 2.28 and 0.83 nm was calculated for 23 and 10 nm films (Figure 11a,b). The resemblances of film morphology with a limited increase in roughness, compared to the as-deposited films, show the structural integrity of the films after the anneal at 500 °C. These results that show NiGe is stable with no phase degradation or agglomeration up to 500 °C are consistent with the previous reports on NiGe films prepared from solid state reaction techniques.[27,16,17,19−21] Studies are underway to test the growth on narrow trenches and evaluate the electrical properties of the integrated NiGe lines. This will be the scope of our future work.

■ CONCLUSION

Ultrathin, high-quality NiGe films were successfully synthesized using a selective solid−vapor reaction of PVD Ni films with GeH_4 gas on 300 mm Si wafers covered with thermal oxides. The GeH_4 chemical vapor reaction conditions (partial pressure, exposure temperature, and time) were optimized for different Ni thicknesses (2−10 nm) to achieve low resistive, stoichiometric, and phase pure NiGe films. Detailed surface analysis shows the onset of NiGe film closure to be >6 nm. NiGe films in the thickness range (10−23 nm) were found to be smooth, uniform, and thermally stable up to 500 °C with a large process window. The films have a sharp interface with a homogeneous composition on thermal oxide substrates and exhibit a resistivity value of 29 $\mu\Omega$ cm for 10 nm NiGe films. The films synthesized using very low temperatures (250−300 °C) and yet demonstrating high quality, despite the absence of adhesion and diffusion barriers, will be beneficial for advanced interconnect applications.

■ AUTHOR INFORMATION

Corresponding Author

*E-mail: anthony.peter@imec.be. Tel.: +32-16-287959. Fax: +32-16-229400.

Notes

The authors declare no competing financial interest.

■ REFERENCES

(1) Aboelfotoh, M. O.; Tawancy, H. M. *J. Appl. Phys.* **1994**, *75* (5), 2441−2446.
(2) Semiconductor Industry Association, *International Technology Roadmap for Semiconductors*: 1999 Edition, pp 163−186.
(3) Hong, S. Q.; Comrie, C. M.; Russel, S. W.; Mayer, J. M. *J. Appl. Phys.* **1991**, *70* (7), 3665−3660.
(4) Wang, Z.; Ramanath, G.; Allen, L. H.; Rockett, A.; Doyle, J. P.; Svensson, B. G. *J. Appl. Phys.* **1997**, *82* (7), 3281−3283.
(5) Liang, H.; Luo, J. S.; Lin, W. T. *Micron* **2002**, *33*, 561−564.
(6) Semiconductor Industry Association, *International Technology Roadmap for Semiconductors*: 2011 Edition, pp 1−94.
(7) Swerts, J.; Arminin, S.; Carbonell, L.; Delabie, A.; Franquet, A.; Mertens, S.; Popovici, M.; Schaekers, M.; Witters, T.; Tokei, Z.; Beyer, G.; Van Elshocht, S.; Gravey, V.; Cockburn, A.; Shah, K.; Aubuchon, J. *J. Vac. Sci. Technol. A* **2012**, *30* (1), 01A1031−01A1035.
(8) Au, Y.; Lin, Y.; Gordon, R. G. *J. Electrochem. Soc.* **2011**, *158* (5), D248−D253.
(9) Chu, J. P.; Lin, C. H.; Sun, P. L.; Leau, D. K. *J. Electrochem. Soc.* **2009**, *156*, H540−H543.
(10) Boragno, C.; Buatier de Mongeot, F.; Felici, R.; Robinson, I. K. *Phys. Rev. B* **2009**, *79*, 155443−155447.
(11) Li, Z.; Rahtu, A.; Gordon, R. G. *J. Electrochem. Soc.* **2006**, *153* (11), C787−C794.
(12) Gadkari, P. R.; Warren, A. P.; Todi, R. M.; Petrova, R. V.; Coffey, K. R. *J. Vac. Sci. Technol. A* **2005**, *23*, 1152−1157.
(13) Kariniemi, M.; Niinisto, J.; Hatanpaa, T.; Kemell, M.; Sajavaara, T.; Ritala, M.; Leskela, M. *Chem. Mater.* **2011**, *23*, 2901−2907.
(14) Chen, L. J. *J. Met.* **2005**, 24−30.
(15) Elbaum, L. K.; Aboelfotoh, M. O. *Appl. Phys. Lett.* **1991**, *58*, 1341−1343.
(16) Park, K.; Lee, B. H.; Lee, D.; Ko, D. H.; Kwak, K. H.; Yang, C. W.; Kim, H. *J. Electrochem. Soc.* **2007**, *154*, H557−H560.
(17) Lee, J. W.; Bae, J. H.; Hwang, J. H.; Kim, H. K.; Park, H.; Yang, C. W. *Microelectron. Eng.* **2012**, *89*, 23−26.
(18) Perrin, C.; Magelinck, D.; Nemouchi, F.; Labar, J.; Lavoie, C.; Bergman, C.; Gas, P. *Mater. Sci. Eng. B* **2008**, *154−155*, 163−167.
(19) Lee, J. W.; Kwak, K. H.; Kim, H.; Yang, C. W. *J. Korean Phys. Soc* **2007**, *50*, 677−680.
(20) Tang, M.; Huang, W.; Cheng, L.; Lai, H.; Chen, S. *IEEE Electron Device Lett.* **2010**, *31*, 863−865.
(21) Zhang, Q.; Wu, N.; Osipowicz, T.; Bera, L. K.; Zhu, C. *Jpn. J. Appl. Phys.* **2005**, *44*, L1389−L1391.
(22) Antony Premkumar, P.; Carbonell, L.; Schaekers, M.; Adelmann, C.; Meersschaut, J.; Franquet, A.; Richard, O.; Bender, H.; Tokei, Z.; Van Elshocht, S. *Intermetallics* **2013**, *34*, 35−42.
(23) Antony Premkumar, P.; Carbonell, L.; Schaekers, M.; Opsomer, K.; Adelmann, C.; Richard, O.; Bender, H.; Franquet, A.; Meersschaut, J.; Wen, L.; Tokei, Z.; Van Elshocht, S. *Microelectron. Eng.* **2013**, http://dx.doi.org/10.1016/j.mee.2013.08.005.
(24) Gaudet, S.; Detavernier, C.; Lavoie, C.; Desjardins, P. *J. Appl. Phys.* **2006**, *100*, 034306-1−034306-10.
(25) Jensen, J.; Sochetra, L.; Johnson, C. *Chem. Mater.* **2003**, *15*, 4200−4204.
(26) Guo, Y.; An, X.; Wang, R.; Zhang, X.; Huang, R. *IEEE Electron Device Lett.* **2011**, *32*, 554−556.
(27) Zhang, Q.; Han, C. W.; Zhu, C. *J. Electrochem. Soc.* **2007**, *154*, H314−H317.
(28) Gaudet, S.; Detavernier, C.; Kellock, A. J.; Lavoie, C.; Desjardins, P.; Lavoie, C. *J. Vac. Sci. Technol. A* **2006**, *24* (3), 474−485.
(29) Zhu, S.; Nakajima, A. *Jpn. J. Appl. Phys.* **2005**, *24*, L753−L755.
(30) Spann, J. Y.; Anderson, R. A.; Thornton, T. J.; Harris, G.; Thomas, S. G.; Tracy, C. *IEEE Electron Device Lett.* **2005**, *26*, 151−153.
(31) Nemouchi, F.; Mangelinck, D.; Labar, J. L.; Putero, M.; Bergman, C.; Gas, P. *Microelectron. Eng.* **2006**, *83*, 2101−2106.
(32) Dellas, N. S.; Minassian, S.; Redwing, J. M.; Mohney, S. E. *Appl. Phys. Lett.* **2010**, *97*, 262116−1−263116−3.
(33) Yan, C. Y.; Higgins, J. M.; Faber, M. S.; Lee, P. S.; Jin, S. *ACS Nano* **2011**, *6*, 5006−5014.
(34) Nash, A.; Nash, P. *Bull. Alloy Phase Diagrams* **1987**, *8*, 255−264.
(35) Liu, Y. Q.; Ma, D. J.; Du, Y. *J. Alloys Compd.* **2010**, *491*, 63−71.
(36) Peng, C. Y.; Huang, C. F.; Yang, Y. J.; Liu, C. W. *ECS Trans.* **2008**, *17*, 249−253.
(37) Jin, L. J.; Pey, K. L.; Choi, W. K.; Fitzgerald, E. A.; Antoniadis, D. A.; Pitera, A. J.; Lee, M. L.; Chi, D. Z.; Tung, C. H. *Thin Solid Films* **2005**, *462−263*, 151.
(38) Massalski, H. *Binary Alloy Phase Diagram*, 2nd ed.; ASN International: Delhi, 1990.
(39) Kang, K.; Gu, G. H.; Kim, D. A.; Park, C. G.; Jo, M. H. *Chem. Mater.* **2008**, *20* (21), 6577−6579.
(40) Zhu, S.; Yu, M. B.; Lo, G. Q.; Kwong, D. L. *Appl. Phys. Lett.* **2007**, *91*, 0519051−0519053.
(41) Brunco, D. P.; Opsomer, K.; de Jaeger, B.; Winderickx, G.; Verheyden, K.; Meuris, M. *Electrochem. Solid State Lett.* **2008**, *11*, H39−H41.
(42) Swerts, J.; Delabie, A.; Salimullah, M. M.; Popovici, M.; Kim, M. S.; Schaekers, M.; Van Elshocht, S. *ECS Solid State Lett.* **2012**, *1*, P19−P21.
(43) Croes, K.; Wilson, C. J.; Lofrano, M.; Beyer, G. P.; Zsolt, T. *Microelectron. Eng.* **2011**, *88*, 614−619.
(44) Gupta, T. *Copper Interconnect Technology*; Springer Science: Berlin, Heidelberg, NY, 2009.

(45) Delavant, M.; Guillan, J.; Galpin, D.; Chhun, S.; Juhel, M.; Guiheux, D.; Jian, P.; Ha, T. H.; Forster, J.; Guggilla, S.; Hong, S.; Bozon, B. *Microelectron. Eng.* **2012**, *92*, 38−41.
(46) Baklanov, M. R.; de Marneffe, J. F.; Shamiryan, D.; Urbanowicz, A. M.; Shi, H.; Rakhimova, T. V.; Huang, H.; Ho, P. S. *J. Appl. Phys.* **2013**, *113*, 041101−41.
(47) Kang, K.; Kim, C. J.; Jo, M. H. *J. Appl. Phys.* **2009**, *105*, 122407−1224011.
(48) Kang, K.; Gu, G. H.; Kim, D. A.; Park, C. J.; Jo, M. H. *Adv. Mater.* **2008**, *20*, 4684−4690.
(49) Park, J. S.; Curtin, M.; Bai, J.; Carroll, M.; Lochtefeld, A. *Jpn. J. Appl. Phys.* **2006**, *45*, 8581−8585.
(50) Ozturk, M. C.; Grider, D. T.; Wortman, J. J.; Littlejohn, M. A.; Zhong, Y. *J. Electron. Mater.* **1990**, *19*, 1129−1134.
(51) Thelander, C.; Agarwal, P.; Brongersma, S.; Eymery, J.; Feiner, L. F.; Forchel, A.; Scheffler, M.; Riess, W.; Ohlsson, B. J.; Gösele, U.; Samuelso, U. *Mater. Today* **2006**, *9*, 28−35.